2011-08

Supramolecular assembly of new heteropolymetalic molecules based on tetraiminodiphenolate macrocycle and hexacyanometallate anions: magnetostructural and spectroscopic properties

Polyhedron, Oxford : Pergamon, v. 30, n. 12, p. 1997-2006, Aug. 2011
http://www.producao.usp.br/handle/BDPI/50084

Polyhedron 30 (2011) 1997–2006

Contents lists available at ScienceDirect

Polyhedron

journal homepage: www.elsevier.com/locate/poly

Supramolecular assembly of new heteropolymetalic molecules based on tetraiminodiphenolate macrocycle and hexacyanometallate anions: Magnetostructural and spectroscopic properties

Rafael Block Samulewski [a], Júlio César da Rocha [a], Rafael Stieler [b], Ernesto Schulz Lang [c], David John Evans [d], Giordano Poneti [e], Otaciro Rangel Nascimento [f], Ronny Rocha Ribeiro [a], Fábio Souza Nunes [a,*]

[a] Departamento de Química, Universidade Federal do Paraná, Cx. Postal 19081, 81531-990 Curitiba, PR, Brazil
[b] Universidade Federal da Fronteira Sul – Campus Realeza, Avenida Rubem Cesar Caselani, no. 3806, 85.770-000 Bairro Cazaca, Realeza, PR, Brazil
[c] Departamento de Química, Universidade Federal de Santa Maria, 97105-900 Santa Maria, RS, Brazil
[d] Department of Biological Chemistry, John Innes Centre, Norwich Research Park, Norwich NR4 7UH, UK
[e] Laboratory of Molecular Magnetism (LAMM), Department of Chemistry, Ugo Schiff and INSTM Research Unit, University of Florence, Via della Lastruccia, 3-13, 50019 Sesto Fiorentino, Florence, Italy
[f] Instituto de Física de São Carlos, Universidade de São Paulo, Cx. Postal 369, 13560-970 São Carlos, SP, Brazil

ARTICLE INFO

Article history:
Received 18 February 2011
Accepted 5 May 2011
Available online 11 May 2011

Keywords:
Dicopper(II)
Tetraiminodiphenolate
Crystal structure
Magnetic measurements
Electronic structure
Supramolecular

ABSTRACT

Herein we report on the synthesis, single crystal X-ray structure, spectroscopic and magnetic properties of $[\{Cu_2(tidf)(H_2O)\}_2(\mu\text{-}CN)_2Fe(CN)_4]\cdot 6H_2O$ **(1)**, $[Cu_2(tidf)(H_2O)_2][Ni(CN)_4]$ **(2)** and $[Cu_2(tidf)(H_2O)_2][Fe(CN)_5NO]\cdot H_2O$ **(3)** (tidf = a Robson type macrocyclic ligand obtained on condensation of 2,6-diformyl-4-methylphenol and 1,3-diaminopropane). Complex **(1)** is pentanuclear; two paramagnetic dicopper(II) units are linked by a hexacyanoferrate(II) ion through two cyano-bridges. All compounds exhibit extensive, three-dimensional, supramolecular structures supported by classic hydrogen bonding between the coordinated aqua ligands, water molecules and cyano groups. Magnetism as a function of the temperature of complexes **1–3** is consistent with a strong antiferromagnetism with exchange parameters 2J estimated −783(29), −913(2), −905(1), respectively.

1. Introduction

Molecules containing paramagnetic metal centers are able to self-assemble through metal-ligand interactions rendering supramolecular assemblies with interesting structural and magnetic properties. This subject is a major challenge in current coordination chemistry [1–5]. Most of these compounds contain two different transition metal ions. Cyanide bridges are linear and suitable to communicate spin density and some compounds behave as high-temperature molecular magnets [6,7]. The study of electronic and magnetic properties is necessary to provide a better understanding of potential metal–metal exchange interactions. These properties are intimately related to the structure and are a result of the nature of the building blocks, their relative orientation in the crystal lattice and interactions such as H-bonding and van der Waals.

In this context, hexacyanometallate anions continue to be intensively investigated as building blocks for the rational design and preparation of heteropolymetallic complexes. These building blocks combined with coordinatively unsaturated systems, like cationic Schiff-bases, produce 1D, 2D or 3D network structures. These assemblies also called Prussian blue analogues gained importance due to the innumerous possibilities to prepare novel extended lattices [8–22].

Robson type ligands, obtained on condensation of 2,6-diformyl-4-methylphenol and diamines, have been investigated over the years as their coordination compounds show interesting magnetic, redox and structural properties [23–36].

Continuing our general interest [2,24–29] in the synthesis of metal complexes of the tetraiminodiphenolate macrocyclic ligand (Scheme 1) we have recently reported the structural, magnetic and spectroelectrochemical properties of the dicobalt complex $[Co_2(tidf)(ClO_4)_2(H_2O)_2]$ [24]. In this work we report on the preparation, characterization and properties of three new heteropolynuclear metal complexes of the Robson family. Our results show a very interesting case of self-assembly of the building molecules into extended structures in the solid state, maintained by intricate hydrogen-bonding interactions. Magnetic and spectroscopic studies are presented as well.

* Corresponding author.
E-mail address: fsnunes@ufpr.br (F.S. Nunes).

0277-5387/$ - see front matter © 2011 Elsevier Ltd. All rights reserved.
doi:10.1016/j.poly.2011.05.001

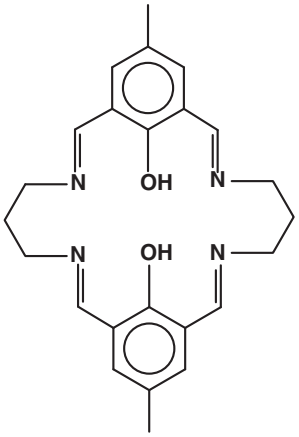

Scheme 1. Ligand tidf.

2. Experimental

2.1. Materials

Reagent grade chemicals were used in this work. $[Cu_2(tidf)(ClO_4)_2(H_2O)_2]$ was prepared as described elsewhere [37].

2.2. Synthesis

2.2.1. $[\{Cu_2(tidf)(H_2O)\}_2(\mu\text{-}CN)_2Fe(CN)_4]\cdot 6H_2O$ (**1**)

$[Cu_2(tidf)(ClO_4)_2(OH_2)_2]$ (0.254 g, 0.33 mmol) was dissolved in 10 mL of acetonitrile and added slowly to 0.07 g (0.167 mmol) of $K_4[Fe(CN)_6]\cdot 3H_2O$ in 12 mL of water/isopropanol (5:1 v/v). After three days dark green crystals were formed, isolated by filtration, washed with water and acetonitrile and dried under vacuum. Yield was 0.22 g (87%). *Anal.* Calc. for $C_{54}H_{80}N_{14}O_{18}Cu_4Fe$ (1523.37 g mol^{-1}): C, 42.54; H, 5.25; N, 12.86. Found: C, 42.60; H, 5.28; N, 12.83%. IR data in cm^{-1}: 2068 (νC≡N, bridge), 2050 and 2026 cm^{-1} (νC≡N, terminal), 1639 ν(C=N), 1573 ν(C=C), 1330 ν(C–O), 671 (νCu–O), 525 (νCu–N).

$[Cu_2(tidf)(H_2O)_2][Ni(CN)_4]$ (**2**) and $[Cu_2(tidf)(H_2O)_2][Fe(CN)_5NO]\cdot H_2O$ (**3**) were prepared as desbribed for **(1)** from equimolar mixtures of $K_2[Ni(CN)_4]\cdot H_2O$ and $Na_2[Fe(CN)_5NO]\cdot 2H_2O$, respectively, with $[Cu_2(tidf)(ClO_4)_2(OH_2)_2]$. Yields were 96% **(2)** and 91% **(3)**. *Anal.* Calc. for $C_{28}H_{30}N_8O_4Cu_2Ni$ (728.39 g mol^{-1}) **(2)**: C, 46.12; H, 4.11; N, 15.37. Found: C, 46.17; H, 4.14; N, 14.76%. IR data in cm^{-1}: 2169, 2164, 2143, 2138 and 2133 (νC≡N), 1639 ν(C=N), 1573 ν(C=C), 1330 ν(C–O), 671 (νCu–O) and 525 (νCu–N). *Anal.* Calc. for $C_{29}H_{32}N_{10}O_6Cu_2Fe$ (799.44 g mol^{-1}) **(3)**: C, 43.53; H, 4.00; N, 17.51. Found: C, 43.63; H, 3.71; N, 18.69%. IR data in cm^{-1}: 2132, 2122 (νC≡N), 1639 ν(C=N), 1573 ν(C=C), 1330 ν(C–O), 671 (νCu–O), 525 (νCu–N).

2.3. Physical measurements

A Bruker CCD X8 Kappa APEX II diffractometer operated using graphite monochromator and Mo Kα radiation (λ = 0.71073 Å) was used for the X-ray structure analyses. The molecular crystal structures were solved by direct methods with SHELXS [38]. The final structure was refined with SHELXL [38] with anisotropic displacement parameters for all non-hydrogen atoms; hydrogen atoms were refined isotropically as riding atoms at their theoretical ideal positions. Drawings were made with the ORTEP-3 for Windows [39]. More detailed information about the structure determinations is given in Table 1.

UV–Vis spectra in the range 190–900 nm were obtained on a VARIAN Cary 100 spectrophotometer in the solid state by diffuse reflectance with a Labsphere® integration sphere. Infrared spectra were obtained with a FTS3500GX Bio-Rad Excalibur series spectrophotometer in the region 4000–400 cm^{-1} in KBr pellets.

The Electron Paramagnetic Resonance (EPR) spectra from powdered solid samples were recorded on a Bruker Elexsys E500 X-band spectrometer and on a Varian E Century Q-band spectrometer. The 77 K spectra were obtained employing a quartz finger Dewar. Spectral simulations were carried out using the EASYSPIN software package [40].

Mössbauer spectra were recorded in zero magnetic field at 80 K on an ES-Technology MS-105 Mössbauer spectrometer with an 89 MBq ^{57}Co source in a rhodium matrix at ambient temperature. Spectra were referenced against a 25 μm iron foil at 298 K and spectrum parameters were obtained by fitting with Lorentzian curves. The magnetic properties of polycrystalline samples of **1–3** have been investigated by SQUID magnetometry using the Cryogenics S600 system. The temperature dependence of the magnetization has been followed in the 1–50 K range with 1 kOe applied field and in the 50–300 K with 10 kOe, while the field dependence of the magnetization were recorded up to 60 kOe at 2 K. The magnetic susceptibility data have been corrected for the diamagnetism of the sample using Pascal constants as well as for the sample holder's contribution.

Microanalyses were done at the Instituto de Química-USP, Brazil.

3. Results and discussion

3.1. Syntheses

The macrocyclic ligand tidf was prepared by the condensation of 2,6-diformyl-4-methylphenol and 1,3-diaminopropane in the presence of magnesium acetate and magnesium nitrate according to the procedure of Nag and co-workers [41].

The magnesium complex $[Mg_2(tidf)](NO_3)_2\cdot 4H_2O$ reacted with copper(II) perchlorate in 1:4 ratio, respectively, to yield 63% of $[Cu(tidf\text{-}H_2)(H_2O)_2](ClO_4)$. This complex reacts with copper(II) perchlorate in a 1:1 proportion, producing the binuclear compound $[Cu_2(tidf)(ClO_4)_2(H_2O)_2]$ as described by Mandal et al. [37]. When treated with $K_4[Fe(CN)_6]\cdot 3H_2O$, $K_2[Ni(CN)_4]\cdot H_2O$ or $Na_2[Fe(CN)_5NO]\cdot 2H_2O$, single crystals of the following polynuclear compounds $[\{Cu_2(tidf)(H_2O)\}_2(\mu\text{-}CN)_2Fe(CN)_4]\cdot 6H_2O$ **(1)**, $[Cu_2(tidf)(H_2O)_2][Ni(CN)_4]$ **(2)** and $[Cu_2(tidf)(H_2O)_2][Fe(CN)_5NO]\cdot H_2O$ **(3)** were formed in very good yields (87–96%) and suitable for crystal structure determination.

The starting materials always reacted in a mixture of polar solvents and in molar ratios that would favor the formation of neutral species and that was the outcome observed in all cases. The compounds are fairly stable and were characterized structurally and spectroscopically as described below.

3.2. Structural description

The complex $[\{Cu_2(tidf)(H_2O)\}_2(\mu\text{-}CN)_2Fe(CN)_4]\cdot 6H_2O$ crystallizes in the triclinic space group *P*-1. Fig. 1 shows the projection of the molecular structure where two units $[Cu_2(tidf)(H_2O)]^{2+}$ are linked by a hexacyanoferrate(II) ion through two cyano-bridges in a *trans* configuration. Copper(II) ions exhibit a square pyramidal geometry with the longest Cu-Cu distance at 9.780 Å and the shortest at 3.133 Å. Also the copper(II) ions are out of the equatorial plane, as seen by the mean deviations from the least-square planes N2N4O1O2 at 0.162(1) Å for Cu2 and N1N3O1O2 at −0.287(1) Å for Cu1. Other main bond distances and angles are Cu1-N5 at

Table 1
Crystal data and structure refinement for complexes **1**, **2** and **3**.

Empirical formula	$C_{54}H_{80}N_{14}O_{18}Cu_4Fe$	$C_{29}H_{32}N_{10}O_6Cu_2Fe$	$C_{28}H_{30}N_8O_4Cu_2Ni$
Formula weight	1523.37	799.44	728.39
T (K)	293(2)	293(2)	293(2)
Radiation, λ (Å)	0.71073	0.71073	0.71073
Crystal system, space group	triclinic, P-1	triclinic, P-1	triclinic, P-1
Unit cell dimensions			
a (Å)	8.2693(2)	10.0764(14)	7.3938(4)
b (Å)	12.6961(3)	12.7160(18)	8.4882(5)
c (Å)	16.7011(5)	12.9909(19	11.5358(7)
α (°)	112.1200(10)	86.998(5)	85.698(2)
β (°)	100.7620(10)	82.847(4)	87.737(3)
γ (°)	92.1910(10)	83.511(4)	78.658(2)
Volume (Å^3)	1584.40(7)	1639.8(4)	707.62
Z, D_{calc} (mg m^3)	2, 1.597	4, 1.619	2, 1.709
Absorption coefficient (mm^1)	1.625	1.780	2.199
F(0 0 0)	788	816	372
Crystal size (mm)	0.179 × 0.145 × 0.08	0.256 × 0.199 × 0.157	0.34 × 0.27 × 0.13
θ Range (°)	1.74–29.70	1.58–28.78	1.77–28.81
Index ranges	$-11 \leqslant h \leqslant 11$	$-13 \leqslant h \leqslant 13$	$-9 \leqslant h \leqslant 9$
	$-17 \leqslant k \leqslant 17$	$-17 \leqslant k \leqslant 17$	$-11 \leqslant k \leqslant 11$
	$-23 \leqslant l \leqslant 23$	$-17 \leqslant l \leqslant 17$	$-15 \leqslant l \leqslant 15$
Reflections collected	31 808	30 645	13 109
Independent reflections	8948 [R_{int} = 0.0444]	8533 [R_{int} = 0.0247]	3660 [R_{int} = 0.0186]
Completeness to θ maximum (%)	99.3	99.6	99.3
Maximum and minimum transmission	1 and 0.8879	1 and 0.9296	0.763 and 0.5219
Absorption correction	GAUSSIAN	GAUSSIAN	GAUSSIAN
Refinement method	full-matrix least-squares on F^2		
Data/restraints/parameters	8948/0/382	8533/0/436	3660/0/196
Goodness-of-fit on F^2	1.035	1.056	1.062
Final R indices [$I > 2\sigma(I)$]	R_1 = 0.0463	R_1 = 0.0264	R_1 = 0.0305
	wR_2 = 0.1137	wR_2 = 0.0711	wR_2 = 0.0754
R indices (all data)	R_1 = 0.0782	R_1 = 0.0314	R_1 = 0.0332
	wR_2 = 0.1297	wR_2 = 0.0741	wR_2 = 0.0741
Largest differences in peak and hole (e Å^3)	1.075 and −0.708	0.755 and −0.513	1.572 and −0.582

Table 2
Selected bond lengths (Å) and angles (°) for complexes **1**, **2** and **3**.

	1	**2**	**3**
Cu–N1	1.986(3)	1.9624(13)	1.9821(17)
Cu–O1	2.006(2)	1.9792(11)	1.9716(14)
Cu–N5	2.214(3)	–	–
Cu–O3	2.367(3)	2.1964(13)	2.2596(16)
N5–C25	1.158(4)	–	–
Fe–C25	1.924(3)	1.9352(18)	–
Cu···Cu	3.133	3.109	3.114
Ni–C14	–	–	1.867(2)
NCuN	97.30(11)	96.54(6)	97.54(7)
C25N5Cu1	135.0(2)	–	–
N5Cu1N1	92.27(11)	–	–
N5Cu1O1	102.60(10)	–	–
$O_{eq}CuN_{eq}$	90.66(10)	92.61(5)	93.02(6)
$O_{axial}CuN_{eq}$	94.78(11)	97.22(5)	92.38(6)
$O_{axial}CuO_{eq}$	101.03(9)	92.66(5)	96.53(6)

2.214(3) Å, Cu2–O3(water) at 2.367(3), Cu1–O1(phenolate) at 2.006(2) Å, Cu2–O1 at 1.972(2) Å, Cu1–N5–C25 at 135.0(2)° and Fe–C25–N5 at 178.6(3)°. Selected bond distances and angles are listed in Table 2.

An extended 1D architecture along the crystallographic axis a is also depicted in Fig. 1. The interactions are through hydrogen bonds such as O4–H4B···N7 at 1.802(3) Å and O4–H4A···N6^i ($i = x - 1, y, z$) at 1.917(3) Å. A complete list of hydrogen distances and angles are in Table 3.

Complexes **2** and **3** also crystallized in the triclinic space group P-1, but in contrast with complex **1**, no cyano-bridge was formed between the metal centers and the building blocks; $[Ni(CN)_4]^{2-}$ and $[Fe(CN)_5(NO)]^{2-}$ acts simply as counter-ions. The unit cell of complex **2** is a CsCl type, with four $[Cu_2(tidf)(H_2O)_2]^{2+}$ in the corners and one $[Ni(CN)_4]^{2-}$ at the center of the cube. The elements of the unit cell are then connected by a 2D hydrogen-bonded supramolecular structure formed through O2–H2A···N3^i (i = $-x + 1$, $-y + 2$, $-z + 1$) at 2.057(2) Å and O2–H2B···N4 at 1.995(2) Å (Fig. 2 and Table 3).

Complex **3** exhibits a complicated structure in which the 3D-order of the crystal depends on the hydrogen-bond interaction between the metallo-complexes and the crystallization water molecule (Fig. 3). The crystallization water molecule is disordered over three positions (O6A, O6B and O6C). The water molecule coordinated to Cu1 is linked simultaneously to the cyano groups C26–N6 and C28–N8 of the nitroprussiate, with bond distances observed for O3–H3A···N6^i (i = $-x + 1$, $-y$, $-z$) at 2.072(2) Å and for O3–H3B···N8^{ii} (ii = $x + 1$, $y - 1$, z) at 2.001(2) Å. The second aqua ligand O4 is coordinated to Cu2 and is connected to one cyano group C25N5 and one water molecule O6A. The hydrogen-bonds observed are O4–H4A···N5 at 1.980(2) Å and O4–H4B···O6A at 1.864(5) Å. The crystallization water molecule is already linked to two cyano groups. The hydrogen-bonds observed are O6C–H6B···N7^{iii} (iii = $x + 1$, y, z) at 1.761(2) Å and O6A–H6A···N9^{iv} (iv = $-x + 1$, $-y + 1$, $-z + 1$) at 1.814(2) Å for the C27N7 and C29N9 of the nitroprussiate, respectively (Table 3).

Thompson and co-workers reported the crystal structure of the dicopper complex $[Cu_2(tidf)(ClO_4)_2(H_2O)_2]$ [37]. The structure has two different molecules in the unit cell, one pseudooctahedral and the other square-pyramidal. Typical bond distances reported for the hexa-coordinated copper are Cu–O(H_2O) at 2.451(9) Å, Cu–O(ClO_4) at 2.589(10), Cu–O(phenoxi) at 1.981(6) Å and Cu–N at 1.956(8).

Andruh and co-workers [42] obtained the iron(III) complex $[Cu_2(tidf)(H_2O)_2]_3[Fe(CN)_6]_2{\cdot}8H_2O$, which contain distinct $[Cu_2(tidf)(H_2O)_2]^{2+}$ and $[Fe(CN)_6]^{3-}$ units. The crystal structure shows three different copper-aqua distances at 2.254(3), 2.280(3) and 2.325(3) Å and the water molecules are connected by hydrogen bonds to the $[Fe(CN)_6]_3^{3-}$ ions. Copper–copper distances are 3.120

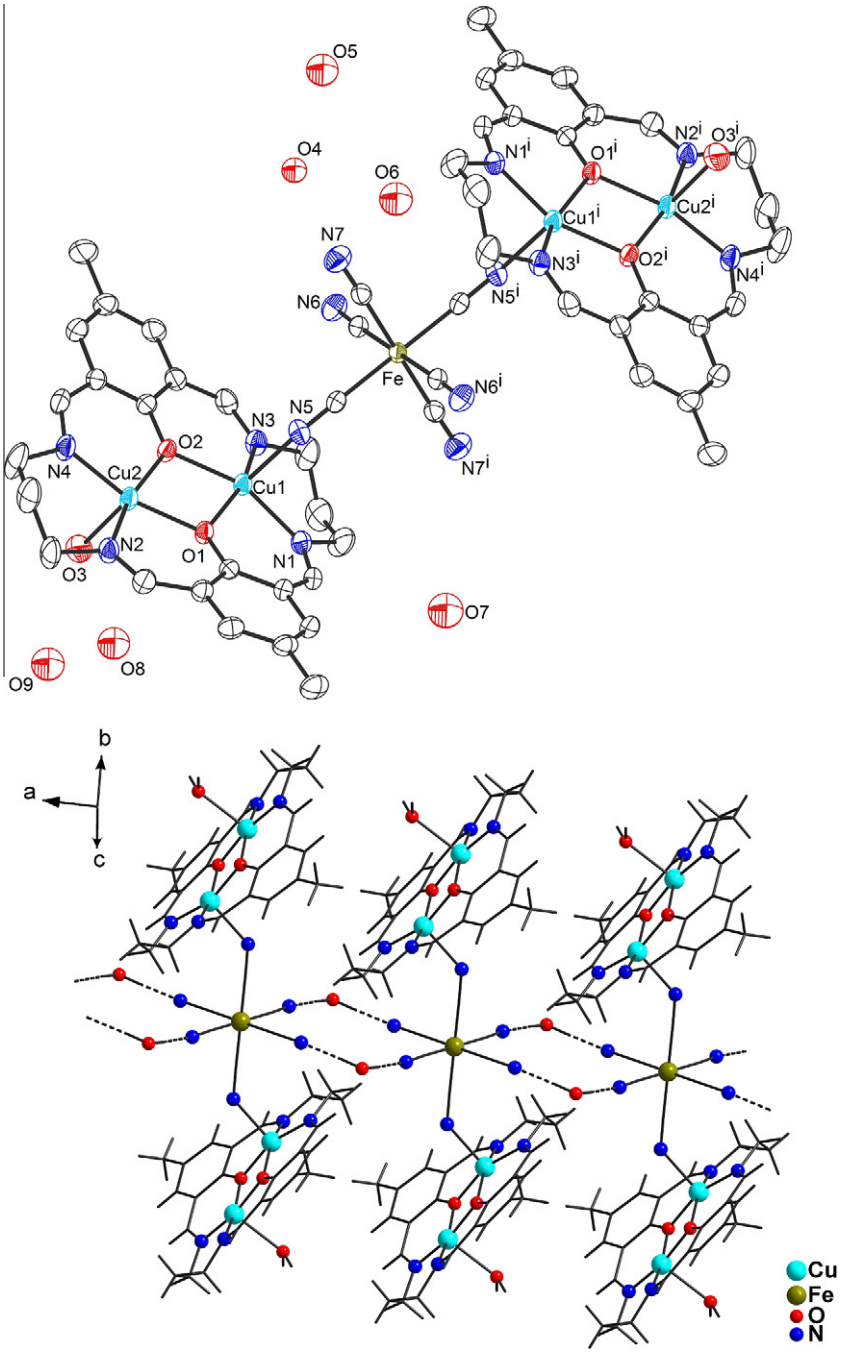

Fig. 1. (Top) View of $[\{Cu_2(tidf)(H_2O)\}_2(\mu\text{-}CN)_2Fe(CN)_4]\cdot 6H_2O$ **(1)** with the atom-labeling scheme and symmetry operations i = 1 − *x*, −*y*, 1 − *z*. Displacement ellipsoids are drawn at the 50% probability level [24]. (Bottom) Extended 1D architecture along the crystallographic axis *a*.

and 3.101 Å, close to the value found in this work and in plane copper–ligand bond lengths are within 1.956–1.997 Å. Two $[Fe(CN)_6]^{3-}$ are linked through hydrogen bonds between two *cis*-cyano ligands to two aqua ligands from two different binuclear units.

More recently Okawa and co-workers [43] described the crystal structures of the complexes $[\{Cu_2(tidf)\}_3\{Cr(oxalate)_3\}_2]\cdot 6MeOH$ and $[\{Cu_2(tidf)\}_3\{Co(CN)_3\}_2]\cdot 6MeOH\cdot 2DMF$. The first crystallizes as a discrete octanuclear unit while the second shows a 2D extended structure.

3.3. Infrared spectra

The vibrational spectrum of complexes **1–3** showed bands also observed in the parent complex $[Cu_2(tidf)(ClO_4)_2(H_2O)_2]$ at 1639 ν(C=N), 1573 ν(C=C) and 1330 ν(C–O), characteristic of the tetraiminodiphenolate macrocycle. The bands at 671 and 525 cm^{-1} were assigned to the vibrational modes νCu–O and νCu–N, respectively. In the νC≡N region, $K_4[Fe(CN)_6]$ exhibited a broad band at 2046 cm^{-1}, while complex **1** showed a splitting with three components at 2068 cm^{-1} (bridge CN^-), 2050 and 2026 cm^{-1} (terminal CN^-) as seen in Fig. 4. The hydrogen bonding through the terminal cyanides seems to be responsible for their asymmetry. Indeed, three different C≡N bonding lengths are observed for the terminal ligands, C25–N5 at 1.159(5), C26–N6 at 1.162(4) and C27–N7 at 1.150(4) Å, in agreement with the splitting pattern observed. A similar behavior was observed for complexes **2** and **3**. Complex **2** exhibited five bands at 2169, 2164, 2143, 2138 and 2133 cm^{-1} and complex **3** two bands at 2132 and 2122 cm^{-1}. Even though

Table 3
Hydrogen-bonding geometric parameters (in Å and °), for complexes **1–3**.

D–H···*A*	*D*–H	H···*A*	*D*···*A*	*D*–H···*A*
Complex ***1***				
O4–H4B···N7	0.929(2)	1.802(3)	2.730(4)	177.23(18)
O4–H4A···N6^{i}	0.910(2)	1.917(3)	2.825(4)	176.00(18)
Complex ***2***				
O2–H2A···N3^{i}	0.8276(16)	2.057(2)	2.883(3)	175.85(12)
O2–H2B···N4	0.8254(15)	1.9951(19)	2.820(2)	176.97(12)
Complex ***3***				
O3–H3A···N6^{i}	0.8826(13)	2.0715(17)	2.932(2)	164.69(9)
O3–H3B···N8^{ii}	0.8452(12)	2.0007(16)	2.845(2)	176.21(11)
O4–H4A···N5	0.8275(11)	1.9803(15)	2.8059(19)	175.34(10)
O4–H4B···O6A	0.8258(12)	1.864(5)	2.677(5)	167.99(18)
O6C–H6B···N7^{iii}	1.045(7)	1.7609(16)	2.773(7)	162.0(4)
O6A–H6A···N9^{iv}	0.986(5)	1.8140(17)	2.798(5)	175.7(3)

(*D* = donor atom, *A* = acceptor atom).
Symmetry codes: complex **1** (i) $x-1, y, z$; complex **2** (i) $-x+1, -y+2, -z+1$; complex **3** (i) $-x+1, -y, -z$; (ii) $x+1, y-1, z$; (iii) $x+1, y, z$; (iv) $-x+1, -y+1, -z+1$.

complexes **2** and **3** do not have any intermetallic cyano-bridge, the network of hydrogen bonds that maintain the supramolecular structures are strong enough to produce vibrational modes with different energies, which account for the observed splittings.

3.4. UV–Vis spectra

Fig. 5 shows the UV–Vis spectrum of a solid sample of complex **1** along with the spectra of the building blocks $[Cu_2(tidf)(ClO_4)_2(H_2O)_2]$ and $K_4[Fe(CN)_6]$ for comparison. The green line represents the spectrum of the pentanuclear complex and it has a close resemblance with that for $[Cu_2(tidf)(ClO_4)_2(H_2O)_2]$ (blue line). The band at 234 nm in complex **1** has both a contribution from $\pi \rightarrow \pi^*$(tidf) and from $d_\pi(Fe^{II}) \rightarrow p_\pi CN$ transitions, as is also seen in the spectrum of $K_4[Fe(CN)_6]$ (red line) [44]. The bands at 337 and 380 are mainly intra-ligand $\pi \rightarrow \pi^*$(tidf) transitions, which are also observed in the spectrum of the free macrocyclic ligand. It is worth mentioning that the bands at 274 and 328 nm in $K_4[Fe(CN)_6]$ are low intensity d–d transitions. A MLCT $d_\pi(Cu^{II}) \rightarrow p_\pi$tidf transition was assigned to the band at 450 nm.

Further, complex **1** also shows a broad structure-less band centered at 672 nm, typical of copper(II) and has contributions from three d–d transitions, $z^2 \rightarrow x^2-y^2$, $xy \rightarrow x^2-y^2$ and $(xz, yz) \rightarrow x^2-y^2$ [45]. This band appears at 605 nm in the binuclear $[Cu_2(tidf)(ClO_4)_2(H_2O)_2]$ complex and reflects the different geometries around the copper(II) ions. The lower energy of the d–d transition for $[Cu_2(tidf)(H_2O)]_2(\mu\text{-}CN)_2Fe(CN)_4]\cdot 6H_2O$ can be explained by considering crystal-field arguments. The Cu–NC and Cu–OH_2 bond lengths are 2.214(3) Å and 2.367(3) Å, respectively. Compare these with the Cu–$OClO_3$ at 2.589(10) Å and Cu–OH_2 at 2.451(9) Å for $[Cu_2(tidf)(ClO_4)_2(H_2O)_2]$ [31]. The closer proximity of the axial ligands, particularly the charged cyanide ligand to the copper(II) in the pentanuclear complex causes the metal ion to come out of the plane of the macrocycle, namely 0.162(1) Å for Cu1 and 0.287(1) Å for Cu2. This weakens the four in plane bonds and overall diminishes the crystal field stabilization energy and the energy of the d–d transition accordingly, as illustrated in the orbital diagram in Scheme 2. This argument is supported by comparison of the in plane Cu–O(phenoxi) and Cu–N bond distances in both complexes. Mean values are Cu–O 2.000 Å and Cu–N 1.971 Å for $[\{Cu_2(tidf)(H_2O)\}_2(\mu\text{-}CN)_2Fe(CN)_4]\cdot 6H_2O$ and, consequently, bigger than the Cu–O 1.981 Å and Cu–N at 1.956 Å for $[Cu_2(tidf)(ClO_4)_2(H_2O)_2]$ [37].

Fig. 6 shows the solid state UV–Vis spectrum for complexes **2** and **3** and their corresponding building blocks. Again, the comparison revealed significant energy changes associated with the geometry around the copper(II) ions upon the reaction between $[Cu_2(tidf)(ClO_4)_2(H_2O)_2]$ and $[Ni(CN)_4]^{2-}$ or $[Fe(CN)_5NO]^{2-}$ ions. In the $[Cu_2(tidf)(ClO_4)_2(H_2O)_2]$ both metal ions are hexacoordinated in a distorted octahedral environment due to Jahn–Teller elongation and the three transitions $z^2 \rightarrow x^2-y^2$, $xy \rightarrow x^2-y^2$ and $(xz, yz) \rightarrow x^2-y^2$ have close energies producing a broad envelope at 605 nm. In complexes **2** and **3**, the copper(II) ions are pentacoordinated and are in a square-pyramidal geometry. Under the crystal field theory approach, this is equivalent of an infinite elongation of one of the axial ligands, reducing the repulsions along the *z* direction. As a result, all three d–d bands are blue-shifted, particularly the transition $(xz, yz) \rightarrow x^2-y^2$, which is shifted to 525 nm as represented in Scheme 2.

3.5. Mössbauer and magnetic properties

The Mössbauer spectrum of $[Cu_2(tidf)(H_2O)]_2(\mu\text{-}CN)_2Fe(CN)_4]\cdot 6H_2O$ was recorded at 80 K and it shows an intense quadrupole split doublet with parameters isomer shift (i.s.) and quadrupole splitting (q.s.) at 0.03 and 0.22 mms^{-1}, respectively, in accordance with a low-spin Fe^{II} configuration. Typical values reported in the literature for $K_4[Fe(CN)_6]\cdot 3H_2O$ are i.s. −0.02 mms^{-1} and q.s. 0.00 mms^{-1} [46]. At 80 K, iron(III) complexes $X_3[Fe(CN)_6]$ gave the following values of i.s. and q.s.: −0.18 and 1.61 mms^{-1} when X is H; −0.04 and 0.47 mms^{-1} for Cs; −0.14 and 0.75 mms^{-1} for Cu. For $K_3[Fe(CN)_6]$ at 298 K the i.s. is −0.124 and q.s. is 0.28 mms^{-1}. At 77 K the q.s. is reported as 0.469 mms^{-1} and the i.s. estimated to be (based on the 298 K i.s. value) −0.024 mms^{-1} [46,47].

The variable-temperature (2–300 K) magnetic measurements were collected for powdered samples of complex **1–3**. The temperature dependence of the molar magnetic susceptibility χ_M along with its product with temperature $\chi_M T$ is displayed in Fig. 7. All of the investigated complexes at 300 K showed $\chi_M T$ values lower than those expected for uncorrelated magnetic centers: complex **1** features a value of 0.53 emu K mol^{-1}, instead of 1.50 emu K mol^{-1}, which is expected for four non interacting Cu^{II} ions; complex **2** showed 0.16 emu K mol^{-1} and complex **3** exhibited 0.15 emu K mol^{-1}, against an expected value of 0.75 emu K mol^{-1}, awaited for the contribution of two uncorrelated Cu^{II} ions.

Moreover, the antiferromagnetic coupling between the copper centers bound to tidf ligand is highlighted by the lowering of the $\chi_M T$ values on decreasing the temperature: the plots related to complexes **2** and **3** move to 0.05 emu K mol^{-1} at 150 K and then reach 0.03 at 50 K. A more complicated behavior is shown by complex **1**, for which the $\chi_M T(T)$ values are higher than in the two previous cases, ranging from 0.53 emu K mol^{-1} at room temperature to 0.34 emu K mol^{-1} at 150 K and finally 0.15 emu K mol^{-1} at 50 K. This behavior has been attributed to a paramagnetic impurity consisting of a non-Curie species present in the measured sample.

In order to evaluate the strength of the magnetic interaction between the copper ions bound to the tidf ligand, a fitting of the magnetic data as function of temperature has been carried out using the Bleaney–Bowers equation, properly modified to take into account paramagnetic impurities present in the samples [48]:

$$\chi_M = (1-\rho)\left(\frac{2Ng^2\beta^2}{k_B T}\right)\left(\frac{1}{3+e^{\frac{2J}{k_B T}}}\right) + \rho\left(\frac{Ng^2\beta^2}{2k_B T}\right) + \mathrm{TIP}$$

Here, ρ is the molar fraction of paramagnetic Cu(II) impurity, g is the Landè factor for Cu(II) (kept fixed at 2.1), β is the Bohr magneton, k_B is the Boltzmann constant and TIP is the sum of the temperature independent paramagnetism contributions of each ion belonging to the different complexes. The TIP values used in the

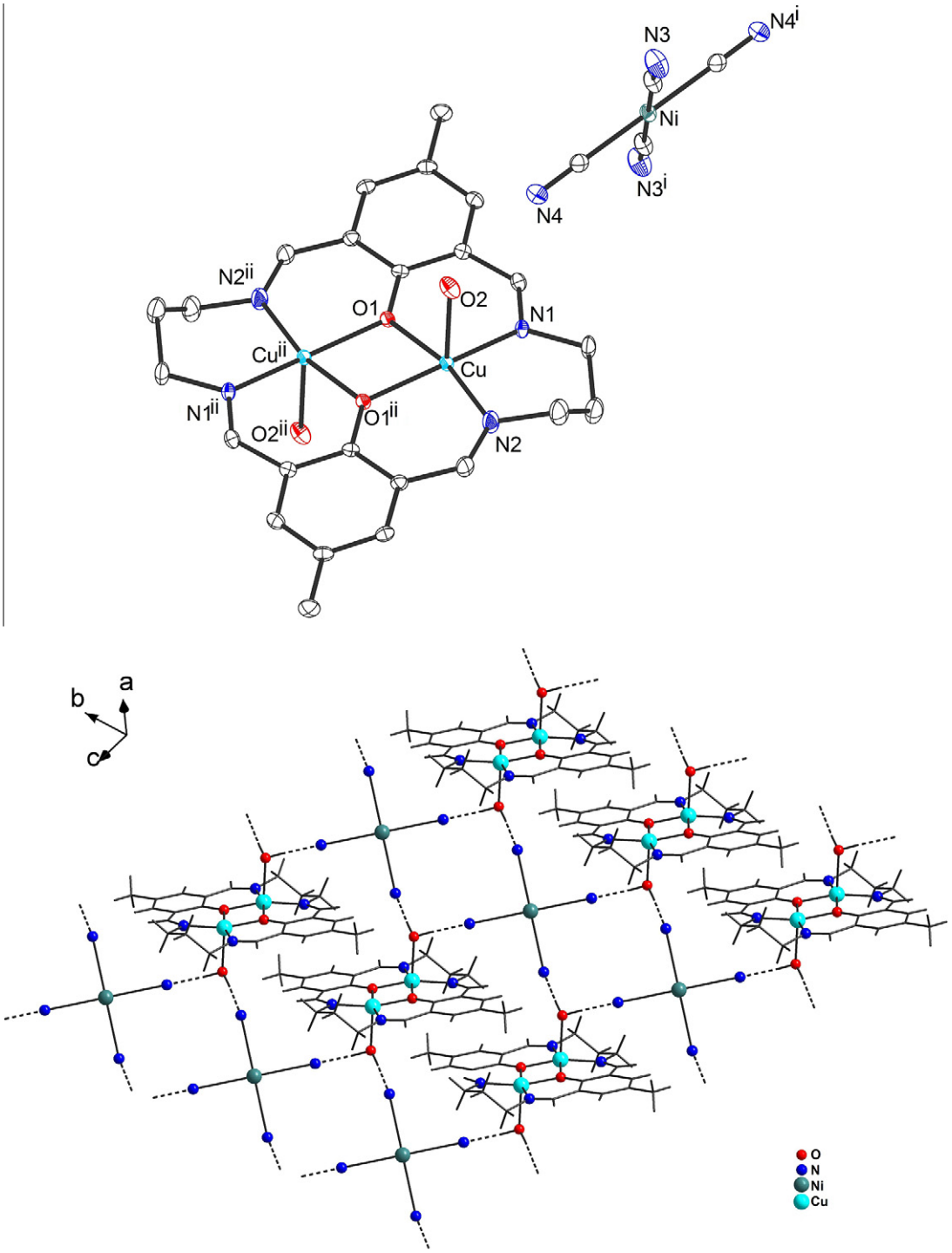

Fig. 2. (Top) View of $[Cu_2(tidf)(H_2O)_2][Ni(CN)_4]$ **(2)** with the atom-labeling scheme and symmetry operations i = 1 − *x*, 3 − *y*, 1 − *z*, ii = 2 − *x*, 2 − *y*, −*z*. Displacement ellipsoids are drawn at the 50% probability level [24]. (Bottom) Extended 2D supramolecular structure formed through hydrogen-bonding.

fit are: 400×10^{-6} emu for complex **1**, 280×10^{-6} emu for **2** and 220×10^{-6} emu for **3**. The $-2J$ energy value corresponds to the energy difference between the triplet and singlet states arising from the isotropic magnetic interaction between the two copper ions bound to the tidf ligand, according to the spin Hamiltonian $H = -2JS_1S_2$. The results of the fitting procedure are shown in the main panel and in the inset of Fig. 7. Best fitting lines shown in Fig. 7 yielded $2J$ values at −783(29), −913(2) and −905(1) cm^{-1} for complexes **1**–**3**, respectively, in accordance with a very strong antiferromagnetic interaction between the copper ions coordinated to the tidf ligand. It must be stressed, however, that the strength of the interactions prevented us from monitoring the magnetism of the systems up to the uncorrelated ions regime, or even to detect the maximum of the $\chi_M(T)$ plots: in this case the extrapolated values for the interaction constant J must be considered as indicative, not quantitative. We attempted for one of the investigated compounds (**1**) to overwhelm the magnetic interaction warming it up to 370 K, but the compound showed a

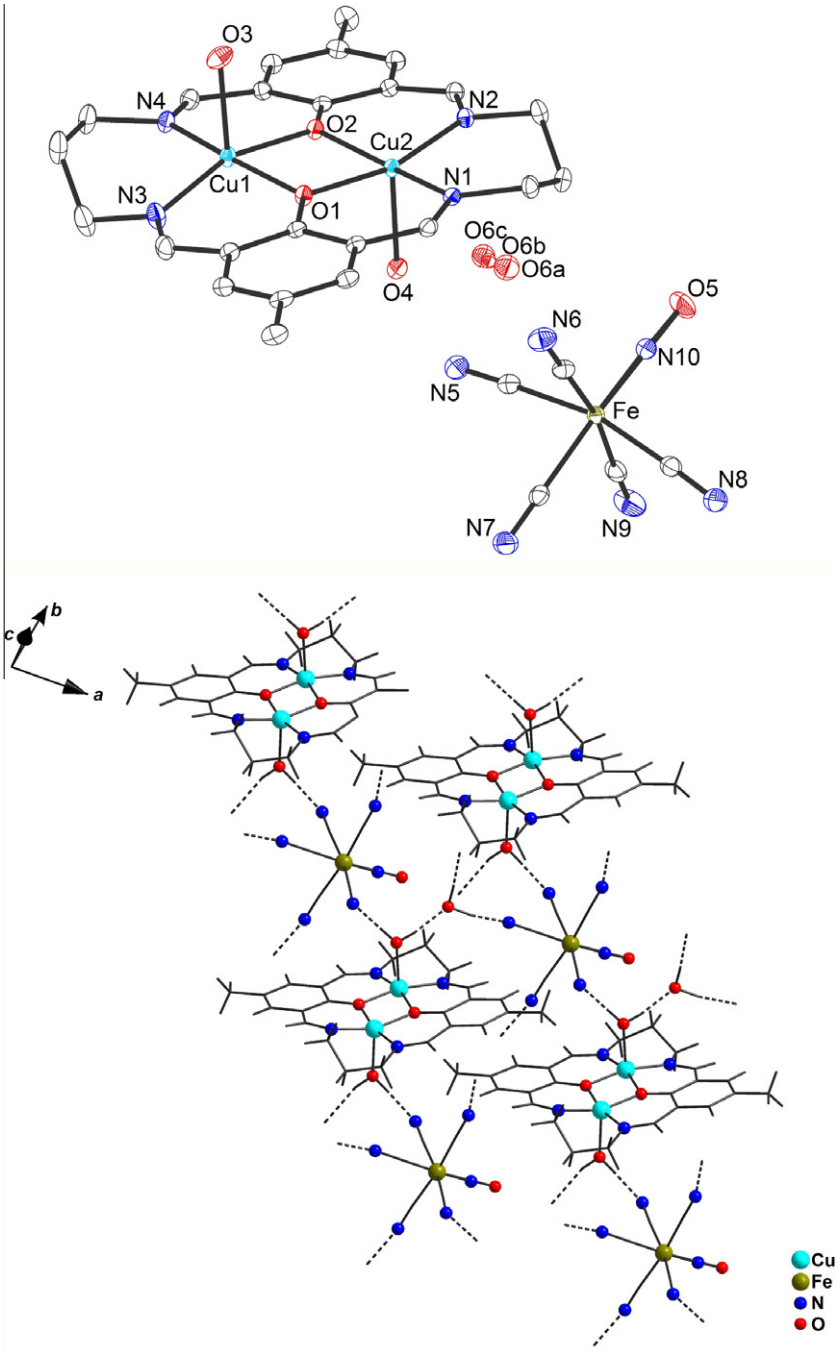

Fig. 3. (Top) View of $[Cu_2(tidf)(H_2O)_2][Fe(CN)_5NO]\cdot H_2O$ **(3)** with the atom-labeling scheme. Displacement ellipsoids are drawn at the 50% probability level [24]. (Bottom) Extended 3D supramolecular structure formed through hydrogen-bonding.

thermally induced irreversible degradation. The observed antiferromagnetic interactions also prevented the observation of three dimensional magnetic ordering of all the investigated compounds.

The observed trend in the magnetic coupling constants shown by compounds **1–3** can be rationalized using structural considerations. The metal ions are connected through the phenolate-bridge and are in close proximity with an average Cu···Cu distance of 3.119 Å. As a consequence, the magnetic properties of these compounds are mainly determined by this intramolecular magnetic exchange that masks the observation of any other phenomenon related to the interaction between copper centers at longer distance. In fact, $[Cu_2(tidf)(H_2O)_2]_3[Fe^{III}(CN)_6]_2\cdot 8H_2O$ does not suffer much influence from the low-spin d^5 iron system and the coupling constant in the binuclear cation $[Cu_2(tidf)(H_2O)_2]^{2+}$, estimated by Andruh and co-workers to be $2J \sim 836\ cm^{-1}$, is practically the same value ($834\ cm^{-1}$) seen for the copper–cobalt complex $[Cu_2(tidf)(H_2O)_2]_3[Co^{III}(CN)_6]_2\cdot 8H_2O$ [42]. Further support to this interpretation is found when the results are compared with the magnetic behavior of the binuclear complex itself, $[Cu_2(tidf)(ClO_4)_2]\cdot H_2O$, which also revealed a $2J$ value of $-850\ cm^{-1}$ [49]. It is interesting to note that complex **1** does show the smallest coupling constant ($J = -783\ cm^{-1}$) when compared to compounds **2**, **3** and all the other cases discussed here. The magnetic coupling seems to be somehow diminished due to the fact that the copper ion is

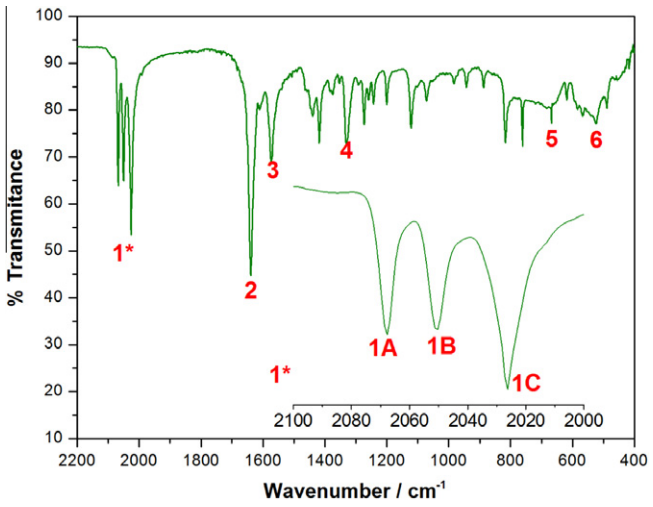

Fig. 4. Infrared spectrum of $[\{Cu_2(tidf)(H_2O)\}_2(\mu\text{-}CN)_2Fe(CN)_4]\cdot 6H_2O$ **(1)** in KBr. Bands 1–6 are at 2068, 1639, 1573, 1330, 671 and 525, respectively.

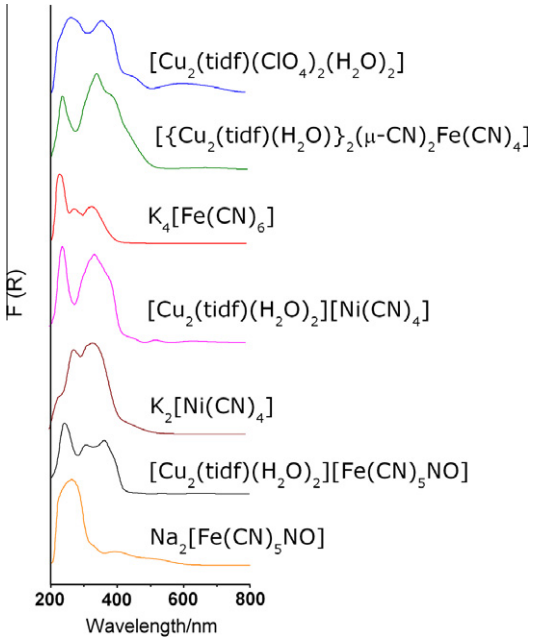

Fig. 5. Diffuse reflectance spectrum of $[\{Cu_2(tidf)(H_2O)\}_2(\mu\text{-}CN)_2Fe(CN)_4]\cdot 6H_2O$ **(1)** and comparison with the building blocks.

displaced out of the plane of the macrocycle as a result of the strong bonding with the cyano-bridge-ligand, an outcome in accord with the short Cu–N bond distance of 2.214(3) Å.

The room temperature X-band EPR spectra of **1**, **2** and **3** (data not shown) are very similar to each other, showing distinctly the presence of Zero Field Splitting (ZFS) arising from mostly dipolar magnetic coupling between the two centers of Cu^{II} in the macrocyclic ligand. However, the X-band spectra were truncated due to the comparable size of the ZFS parameter D and the X-band photon energy ($D \sim h\nu$), which discouraged any simulation of those spectra and demanded higher energy EPR spectroscopy for the purpose of parameter determination.

Fig. 8 shows the Q-band EPR room temperature spectrum of **2**. The spectrum consists of a dipolar pattern with prominent perpendicular turning points at 1.0 T and 1.3 T and one of the parallel at 0.75 T. The second parallel turning point is not shown due to

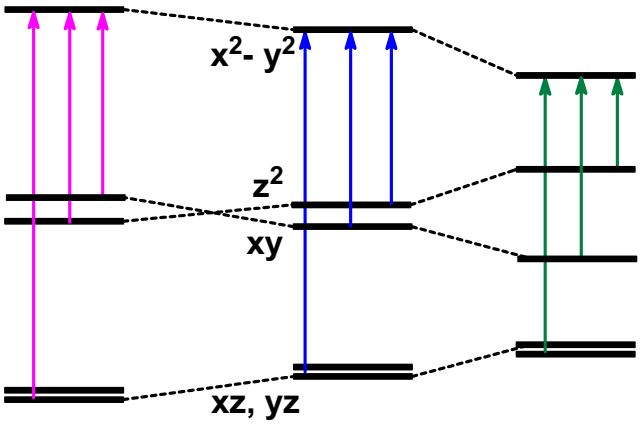

Scheme 2. Crystal-field orbital splittings of $[\{Cu_2(tidf)(H_2O)\}_2(\mu\text{-}CN)_2Fe(CN)_4]\cdot 6H_2O$ **(1)**, $[Cu_2(tidf)(H_2O)_2][Ni(CN)_4]$ **(2)** and $[Cu_2(tidf)(ClO_4)_2(H_2O)_2]$.

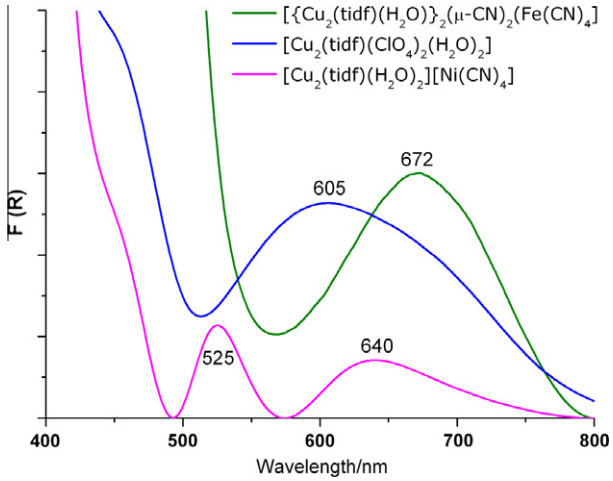

Fig. 6. Low-energy bands of $[\{Cu_2(tidf)(H_2O)\}_2(\mu\text{-}CN)_2Fe(CN)_4]\cdot 6H_2O$ **(1)**, $[Cu_2(tidf)(H_2O)_2][Ni(CN)_4]$ **(2)** and $[Cu_2(tidf)(ClO_4)_2(H_2O)_2]$.

instrumental upper magnetic field limit. The spectrum also shows a half field transition at *ca.* 0.5 T, which corresponds to a $\Delta m_S = \pm 2$ transition.

The simulated g-tensor is practically axial, consistent with the square base pyramid molecular geometry of the two Cu^{II} centers (cf. Table 4). The unfitted central portion (*ca.* $g = 2$) of the spectrum corresponds to naturally occurring mononuclear Cu^{II} species.

The expected value for the ZFS parameter D for a pure dipolar splitting is *ca.* 0.1 cm^{-1}, which corresponds to an inter Cu^{II} distance of 3.119 Å. The observed difference corresponds to the influence of spin orbit coupling and anisotropic exchange interaction, which may also, explains the rhombicity of the observed ZFS tensor reflected in the simulated E parameter (Table 4) [50].

The 77 K spectra of **1**, **2** and **3** (data not shown) do not show the dipolar splitting observed at room temperature, in agreement to the antiferromagnetic behavior determined by direct susceptibility measurements.

4. Conclusion

Three new compounds were prepared ($[\{Cu_2(tidf)(H_2O)\}_2(\mu\text{-}CN)_2Fe(CN)_4]\cdot 6H_2O$ **(1)**, $[Cu_2(tidf)(H_2O)_2][Ni(CN)_4]$ **(2)** and $[Cu_2(tidf)(H_2O)_2][Fe(CN)_5NO]\cdot H_2O$ **(3)**) and their structure analyzed. They all show a complex supramolecular structure sustained by hydrogen-bond interactions. The molecular magnetism exhibited

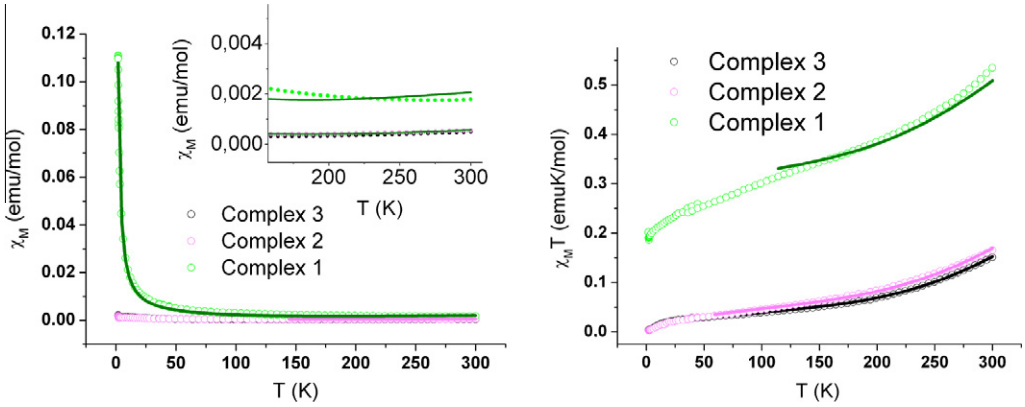

Fig. 7. Magnetic susceptibility as a function of the temperature for $[\{Cu_2(tidf)(H_2O)\}_2(\mu\text{-}CN)_2Fe(CN)_4]\cdot 6H_2O$ (**1**), $[Cu_2(tidf)(H_2O)_2][Ni(CN)_4]$ (**2**) and $[Cu_2(tidf)(H_2O)_2][Fe(CN)_5NO]\cdot H_2O$ (**3**). The solid line is the best fit according to the theoretical expression discussed in the text.

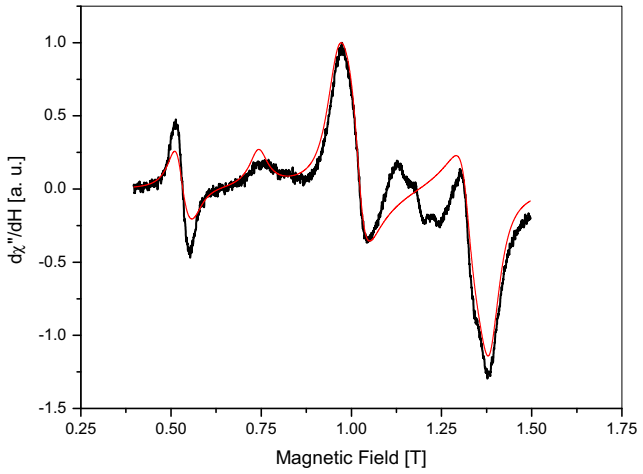

Fig. 8. Room temperature Q-band EPR spectrum of sample $[Cu_2(tidf)(H_2O)_2][Ni(CN)_4]$ (**2**) and simulation (red) (Colour online).

Table 4
EPR simulation parameters for Q-band room temperature spectrum of complex **2**.

gx	*gy*	*gz*	*D* [cm^{-1}]	*E* [cm^{-1}]
2.063100	2.060623	2.299823	0.34405	0.0178

by complexes **1–3** are essentially a result of a strong exchange coupling between magnetic orbitals of the copper(II) ions bridged by the phenolate bridge within the macrocyclic unit. The strong coordination of the cyanide ligand to the copper ion causes a structure distortion as the metal comes out of the plane of the tidf ligand, resulting in a short bond distance and a significant decrease of the magnetic exchange coupling. The electronic structure of the compounds is sensitive to the geometry around the copper and the spectra can be correlated with the degree of tetragonal distortions.

Acknowledgements

F.S.N., R.B., J.C.R. and E.S.L. thank CNPq for research fellowships. Diffractometer was supported by the Financiadora de Estudos e Projetos (FINEP, CT-Infra 03/2001). DJE thanks the Biotechnology and Biological Sciences Research Council, UK, for funding. We also thank Dr. Jaísa Fernandes Soares (DQ-UFPR) for the magnetic measurements.

Appendix A. Supplementary data

CCDC 788666, 790197 and 790198 contains the supplementary crystallographic data for this paper. These data can be obtained free of charge via http://www.ccdc.cam.ac.uk/conts/retrieving.html, or from the Cambridge Crystallographic Data Centre, 12 Union Road, Cambridge CB2 1EZ, UK; fax: (+44) 1223-336-033; or e-mail: deposit@ccdc.cam.ac.uk.

References

[1] B.K. Tripuramullu, R. Kishore, S.K. Das, Polyhedron 29 (2010) 2985.
[2] K.V. Shuvaev, L.N. Dawe, L.K. Thompson, Eur. J. Inorg. Chem. (2010) 4583.
[3] K.B. Shiu, S.A. Liu, G.H. Lee, Inorg. Chem. 49 (2010) 9902.
[4] O.Z. Yesiel, H. Erer, G. Kastas, I. Kani, Polyhedron 29 (2010) 2600.
[5] H.A. Habib, B. Gil-Hernandez, K. Abu-Shandi, J. Sanchiz, C. Janiak, Polyhedron 29 (2010) 2537.
[6] T. Mallah, S. Thiebaut, M. Verdaguer, P. Veillet, Science 262 (1993) 1554.
[7] W.R. Entley, G.S. Girolami, Science 268 (1995) 397.
[8] M. Atanasov, P. Comba, S. Hausberg, B. Martin, Coord. Chem. Rev. 253 (2009) 2306.
[9] F.H.O. Ishiruji, N.L. Speziali, M.G.F. Vaz, F.S. Nunes, J. Braz. Chem. Soc. 21 (2010) 1195.
[10] R. Podgajny, T. Korzeniak, P. Przychodzen, C. Gimenez-Saiz, M. Ramns, M. Kwasniak, B. Sieklucka, Eur. J. Inorg. Chem. (2010) 4166.
[11] A. Bienko, K. Suracka, J. Mrozinski, R. Kruszynski, D. Bienko, A. Wojciechowska, R. Boca, Polyhedron 29 (2010) 2546.
[12] D.Y. Wu, Y.J. Zhang, W. Huang, O. Sato, Dalton Trans. 39 (2010) 5500.
[13] J.F. Guo, X.T. Wang, B.W. Wang, G.C. Xu, S. Gao, L. Szeto, W.T. Wong, W.Y. Wong, T.C. Lau, Chem.-A Eur. J. 16 (2010) 3524.
[14] H. Higashikawa, K. Inoue, K.Y. Maryunina, G.V. Romanenko, A.S. Bogomyakov, O.V. Kuznetsova, E.Y. Fursova, V.I. Ovcharenko, J. Struct. Chem. 50 (2009) 1155.
[15] F.H.O. Ishiruji, D.J. Evans, F.L. Benedito, F.S. Nunes, Spectrochim. Acta A 70 (2008) 1029.
[16] L.J. Cavichiolo, M. Hörner, E.R. Crespan, M.G.F. Vaz, D.J. Evans, F.S. Nunes, Z. Anorg. Allg. Chem. 634 (2008) 1613.
[17] W.-T. Chen, G.-C. Guo, M.-S. Wang, G. Xu, L.-Z. Cai, T. Akitsu, M. Akita-Tanaka, A. Matsuhita, J.-S. Huang, Inorg. Chem. 46 (2007) 2105.
[18] M. Shatruk, A. Dragulescu-Andrasi, K.E. Chambers, S.A. Stoian, E.L. Bominaar, C. Achim, K.R. Dunbar, J. Am. Chem. Soc. 129 (2007) 6104.
[19] A. Rodríguez-Diéguez, R. Kivekäs, H. Sakiyama, A. Debdoubi, E. Colacio, Dalton Trans. (2007) 2145.
[20] P.V. Bernhardt, F. Bozoglian, G. Gonzalez, M. Martizez, B.P. Macpherson, B. Sienra, Inorg. Chem. 45 (2006) 74.
[21] M. Atanasov, P. Comba, S. Förster, G. Linti, T. Malcherek, R. Miletich, A.I. Prikhod'ko, H. Wadepohl, Inorg. Chem. 45 (2006) 7722.
[22] C. Paraschiv, M. Andruh, Y. Journaux, Z. Zak, N. Kyritsakas, L. Ricard, J. Mater. Chem. 16 (2006) 2660.
[23] R. Robson, N.H. Pilkington, Aust. J. Chem. 23 (1970) 2225.
[24] R.B. Samulewski, Júlio C. da Rocha, O. Fuganti, R. Stieler, E.S. Lang, M.G.F. Vaz, F.S. Nunes, J. Mol. Struct. 984 (2010) 354.
[25] A.R. Raimondi, D.J. Evans, F.S. Nunes, Spectrochim. Acta A 70 (2008) 651.
[26] A.R. Raimondi, D.J. Evans, S.M. Drechsel, T. Hasegawa, F.S. Nunes, Spectrochim. Acta A 67 (2007) 145.

[27] A.C. Raimondi, T. Hasegawa, D.J. Evans, Spectrochim. Acta 61 (2005) 1929.
[28] A.C. Raimondi, P.B. Hitchcock, G.J. Leigh, F.S. Nunes, J. Chem. Cryst. 34 (2004) 83.
[29] A.C. Raimondi, A.S. Mangrich, V.S. Franco, H.E. Toma, F.S. Nunes, Polyhedron 23 (2004) 2069.
[30] A.C. Raimondi, P.B. Hitchcock, G.J. Leigh, F.S. Nunes, J. Chem. Cryst. 32 (2002) 363.
[31] L.K. Thompson, S.K. Mandal, S.S. Tandon, J.N. Bridson, M.K. Park, Inorg. Chem. 35 (1996) 3117.
[32] R.R. Gagné, C.L. Spiro, T.J. Smith, C.A. Hamann, W.R. Thies, A.K. Shiemke, J. Am. Chem. Soc. 103 (1981) 4073.
[33] C.L. Spiro, L.L. Lambert, T.J. Smith, E.N. Duesler, R.R. Gagné, D.N. Hendrickson, Inorg. Chem. 20 (1981) 1229.
[34] R.R. Gagné, L.M. Henling, T.J. Kistenmacher, Inorg. Chem. 19 (1980) 1226.
[35] S.L. Lambert, D.N. Hendrickson, Inorg. Chem. 18 (1979) 2683.
[36] H. Okawa, S. Kida, Bull. Chem. Soc. Jpn. 45 (1972) 1759.
[37] S.K. Mandal, L.K. Thompson, M.J. Newlands, E.J. Gabe, Inorg. Chem. 28 (1989) 3707.
[38] G.M. Sheldrick, Acta Crystallogr., Sect. A 64 (2008) 112.
[39] L.J. Farrugia, J. Appl. Cryst. 30 (1997) 565.
[40] S. Stoll, A. Schweiger, J. Magn. Reson. 178 (2006) 42.
[41] S. Mohanta, K.K. Nanda, S. Ghosh, M. Mukherjee, M. Heliwell, K. Nag, J. Chem., Dalton Trans. (1996) 4233.
[42] G. Grasa, F. Tuna, R. Gheorghe, D.B. Leznoff, S.J. Rettig, M. Andruh, N. J. Chem. 24 (2000) 615.
[43] Y. Miyazato, M. Ohba, H. Okawa, Bull. Chem. Soc. Jpn. 78 (2005) 1646.
[44] H.B. Gray, N.A. Beach, J. Am. Chem. Soc. 85 (1963) 2922.
[45] G. Protasiewyck, F.S. Nunes, Spectrochim. Acta A 65 (2006) 549.
[46] N.N. Greenwood, T.C. Gibb, Mossbauer Spectroscopy, Chapman and Hall Ltd., London, 1971.
[47] W.T. Oosterhuis, G. Lang, S. DeBenedetti, Phys. Lett. 24A (1967) 346.
[48] O. Kahn, Magnetochemistry, VCH, New York, 1993.
[49] S. Mohanta, B. Adhikary, S. Baitalik, K. Nag, New J. Chem. 25 (2001) 1466.
[50] A. Bencini, D. Gatteschi, Electron Paramagnetic Resonance of Exchange Coupled Systems, Springer-Verlag, Berlin, Heidelberg, 1990. pp. 75–76.